Paticle-in-Cell Simulation of a Micro ECR Plasma Thruster

IEPC-2015-240／ISTS-2015-b-240

Presented at Joint Conference of 30th International Symposium on Space Technology and Science
34th International Electric Propulsion Conference and 6th Nano-satellite Symposium,
Hyogo-Kobe, Japan
July 4 – 10, 2015

Keisuke Ueno[1], Daisuke Mori, Yoshinori Takao, Koji Eriguchi[2], and Kouichi ONO[3]
Department of Aeronautics and Astronautics, Graduate School of Engineering,
Kyoto University, Katsura, Nishikyo-ku, Kyoto, 615-8540, Japan

Abstract: Two-dimensional axisymmetric particle-in-cell simulations with a Monte Carlo collision algorithm have been conducted for the numerical analysis for a micro ECR plasma thruster. The thruster consisted of a rod antenna and a microplasma chamber surrounded by axially magnetized rings. Numerical results with 4-GHz microwaves and 0.143-T magnetic fields indicated that ions generated in the plasma are well confined by the applied magnetic field and the ions are accelerated through divergent magnetic fields. We also verified the ECR effect in the discharge tube area.

Nomenclature

B_{ECR}	=	resonant magnetic field for ECR
B_{rem}	=	remanent magnetic flux density
B_z	=	axial magnetic flux density at $r = 0$
k	=	Boltzmann constant
n_{n}	=	neutral density
σ_{T}	=	cross section
l	=	half length of ring magnet
n	=	ion or electron density
ρ	=	charge density
μ_0	=	permeability of vacuum
ε_0	=	permittivity of vacuum
q	=	elementary charge
R_1	=	inner radius of ring magnet
R_2	=	outer radius of ring magnet
r	=	outer radius of ring magnet
z	=	axial position
$\boldsymbol{E}$	=	electric field (vector)
$\boldsymbol{B}$	=	magnetic field (vector)
$\boldsymbol{j}$	=	plasma current (vector)
A	=	cross section
$\boldsymbol{v}$	=	ion or electron velocity (vector)

---

[1] Graduate Student, Department of Aeronautics and Astronautics, Email: ueno.keisuke.65m@st.kyoto-u.ac.jp.
[2] Associate Professor, Department of Aeronautics and Astronautics, Email: eriguchi@kuaero.kyoto-u.ac.jp.
[3] Professor, Department of Aeronautics and Astronautics, Email: ono@kuaero.kyoto-u.ac.jp.

I. Introduction

In recent years, a small-scale spacecraft has been actively developed in laboratories and companies around the world, which is inspired by the demands for reducing all mission costs and increasing launch rates. Then, propulsion systems should be downsized for the miniaturized spacecraft, to meet the requirements for a higher-precise station keeping and attitude control. In addition, in order to operate microthrusters for a long time, the durability and low-power consumptions are required.

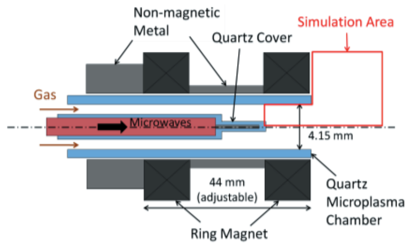

Figure 1. Cross sectional view of the micro ECR plasma thruster.

In this background, we have studied electromagnetic microthrusters using electron cyclotron resonance (ECR) discharges[1]. We developed a new type of the thruster shown in Fig. 1, which has a feature of electrodeless, simple structure. The microthruster consists of a 4.15-mm-diam. quartz microplasma chamber surrounded by permanent magnet rings and a microwave antenna covered with a quartz envelope. The plasma is generated by 4-GHz microwaves of < 10 W in magnetic fields of 0.143 T with a propellant gas of Xe, where the ions are accelerated through divergent magnetic fields and the resulting ambipolar electric fields generated[2,3].

In order to increase the thrust performance, it is necessary to increase the electron density in the discharge tube area. In our previous work, the electron density was measured to be of the order of 10^{16} m^{-3} in the discharge tube area of our thruster, but this value is too low for control of the attitude of a small-scale spacecraft[1]. For improving the electron density, it is crucial to understand micro plasma characteristics more profoundly. In order to understand the micro ECR plasma of our thruster, we verified the ECR effect, the confinement of the plasma, and the acceleration of ions in divergent magnetic fields.

II. Numerical Model

Figure 2 shows the simulation area, consisting of a discharge tube area and out-of-discharge tube area, which is divided into square cells with a grid spacing of 0.1 mm.

To investigate the characteristics of the plasma of the micro ECR thruster, we conducted two-dimensional axisymmetric particle-in-cell simulations with a Monte Carlo collision algorithm (PIC/MCC). The present PIC/MCC model consists of the electromagnetic equation for the induced electric field by the coaxial cable, the Poisson equation for the electrostatic field due to the space charge, the equation of motion, and collisions of charged particles. The flowchart of the calculation is shown in Fig. 3. The time steps of ion and electron are 2.5×10^{-10} s (one microwave cycle) and 1.25×10^{-11} s, respectively. A number of simulation superparticles (singly ionized xenon ions and electrons) are loaded in two-dimensional spatial computational meshes (r,z), with three velocity components (v_r, v_θ and v_z). As an initial condition, ions and electrons are set in the plasma generation area (Fig. 2) with a density of 1×10^{16} m^{-3} (the initial ion and electron temperatures are 0.2 and 5.0 eV, respectively, with the velocity distributions being Maxwellian); then, after starting the calculation, particles continue to be given in the plasma generation area at each time step to keep the plasma generation area spatially uniform (1×10^{16} m^{-3}). In a previous work, the electron density in the discharge tube area was measured by a cylindrical Langmuir probe, being on the order of 1×10^{16} m^{-3} [1].

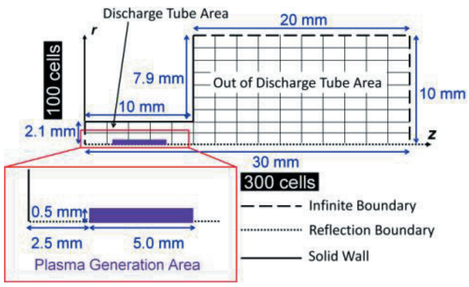

Figure 2. Simulation area.

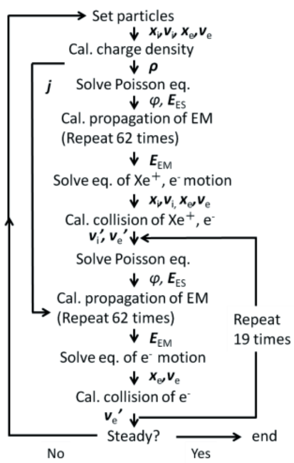

Figure 3. Flowchart of the calculation.

The equation of motion for charged particles is solved explicitly by the time-centered leap frog method for the time integration and the Buneman-Boris method for the velocity advance with a coordinate rotation for the position advance. The PIC-FDTD unit cell is shown in Fig. 4 for the cylindrical coordinates, which is similar to the Yee's rectangular coordinate cube cell. The components of the electric $\boldsymbol{E}$ and magnetic $\boldsymbol{B}$ fields are located on the cell, together with the current density $\boldsymbol{j}$ induced. The size of the cell is taken to be Δr and Δz in the r and z direction, respectively, where Δr and Δz are taken to be both 0.1 mm. The electrostatic field $\boldsymbol{E}_{\mathrm{ES}}$ is given by

$$\boldsymbol{E}_{\mathrm{ES}} = -\nabla\varphi, \tag{1}$$

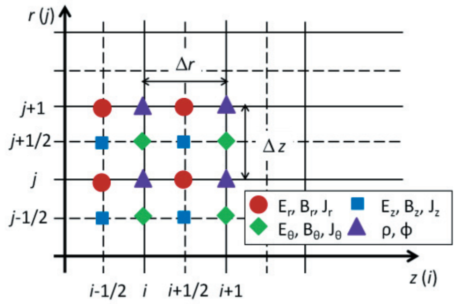

Figure 4. PIC unit cell and FDTD unit cell in the cylindrical coordinates, where Δr and Δz are both 0.1 mm.

where the potential φ is derived from the space charge of charged particles. The Poisson equation is given by

$$\left(\frac{\partial^2}{\partial r^2} + \frac{1}{r}\frac{\partial}{\partial r} + \frac{\partial^2}{\partial z^2}\right)\varphi = -\frac{\rho(r,z)}{\varepsilon_0}. \tag{2}$$

Equation (2) is solved by using the method of successive-over-relaxation (SOR). The potential is assumed to be zero at the wall of the quartz tube and magnet. The electrostatic field is determined by the central difference from the potential. The propagation of electromagnetic waves is calculated by Maxwell's equations:

$$\frac{1}{\mu_0}(\nabla \times \boldsymbol{B}_{\mathrm{EM}}) = \boldsymbol{j} + \varepsilon_0\frac{\partial \boldsymbol{E}_{\mathrm{EM}}}{\partial t}, \tag{3}$$

$$(\nabla \times \boldsymbol{E}_{\mathrm{EM}}) = -\frac{\partial \boldsymbol{B}_{\mathrm{EM}}}{\partial t}, \tag{4}$$

$$\boldsymbol{j} = qn\boldsymbol{v}. \tag{5}$$

Under the assumption of $\partial/\partial\theta = 0$, only the transverse magnetic (TM) waves exist in the azimuthally symmetric configuration with $\boldsymbol{E} = (E_r, 0, E_z)$ and $\boldsymbol{B} = (0, B_\theta, 0)$[4]. Equations (3) – (5) are solved by using the finite-difference time-domain (FDTD) approximation with a time increment $\Delta t_{\mathrm{FDTD}} = 2.0\times10^{-13}$ s (1/1250 of the microwave cycle). The transverse electromagnetic (TEM) waves are given to the system at the excitation plane (z = 0, r = 0.3 ~ 0.8 mm) with the total power injection, which of 1.0 W into the discharge tube area, which is monitored at z = 1.0 mm by using

$$P_{\mathrm{in}} = \frac{1}{\mu_0}\int_{\mathrm{A}} (\boldsymbol{E}\times\boldsymbol{B})\cdot d\boldsymbol{A}. \tag{6}$$

At the outer edge of the out-of-discharge tube area and the excitation plane, Mur's first order absorbing boundary conditions,

$$\frac{\partial E_{\mathrm{r}}}{\partial z} \pm \frac{1}{c}\frac{\partial E_{\mathrm{r}}}{\partial t} = 0, \tag{7}$$

$$\frac{\partial E_{\mathrm{z}}}{\partial r} + \frac{1}{c}\frac{\partial E_{\mathrm{z}}}{\partial t} = 0, \tag{8}$$

are applied to field components E_r and E_z, where the wall is assumed to be a conducting wall[5].

Summing up $\boldsymbol{E}_{\mathrm{ES}}$ and $\boldsymbol{E}_{\mathrm{EM}}$, we can obtain the electric field and renew the velocity of particles by using the equation of motion:

$$\frac{\mathrm{d}\boldsymbol{v}}{\mathrm{d}t} = \frac{q}{m}(\boldsymbol{E}_{\mathrm{ES}} + \boldsymbol{E}_{\mathrm{EM}} + \boldsymbol{v} \times \boldsymbol{B}_{\mathrm{st}}), \tag{9}$$

where, only the magnetostatic fields $\boldsymbol{B}_{\mathrm{st}}$ of the permanent magnet is taken into account (the magnetic fields of microwaves are negligibly small as compared with $\boldsymbol{B}_{\mathrm{st}}$)[6].

The intensity of the magnetic flux density is required to satisfy the ECR condition, B_{ECR}, = 0.143 T for 4-GHz microwaves. The axial magnetic field along the axis of an axially magnetized ring is given by

$$B_z(z) = \frac{B_{\mathrm{rem}}}{2}\left[\left(\frac{z+l}{\sqrt{(z+l)^2+R_2^2}} - \frac{z-l}{\sqrt{(z-l)^2+R_2^2}}\right) - \left(\frac{z+l}{\sqrt{(z+l)^2+R_1^2}} - \frac{z-l}{\sqrt{(z-l)^2+R_1^2}}\right)\right], \tag{10}$$

where the origin of axial position is the midpoint of the ring magnet [7]. Figure 5 shows the axial magnetic field at the centerline of the plasma chamber generated by the two magnets as a function of axial position, which was calculated based on eq. (10). In this figure, the axial position $z = 0$ denotes the midpoint between two magnets. In order to obtain the magnetostatic fields distribution, we performed the two-dimensional, axially-symmetric static magnetic field analysis with ANSYS software. Figure 6 shows the contour of the magnetic flux density.

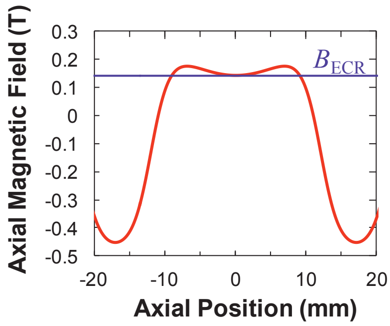

Figure 5. Axial magnetic field as a function of axial position in the discharge tube area. The origin of axial position is set at the midpoint between two magnets.

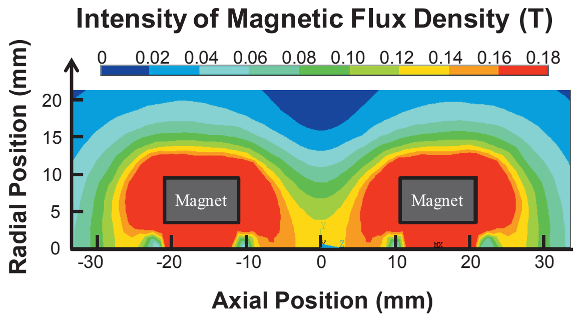

Figure 6. Contour of the magnetic flux density around two ring magnets, analyzed by ANSYS software.

In these simulations, the collisions are described by the null-collision method to reduce the calculation time[8]. In this method, the number of collisions at each time step is determined by the maximum collision frequency, as

$$\nu' = \max(n_{\mathrm{n}})\max(\sigma_{\mathrm{T}} v). \tag{11}$$

From the maximum collision frequency, we can determine the probability P of occurring collisions by

$$P = 1 - \exp(-\nu' \Delta t). \tag{12}$$

From P, we can determine the number of times $Nc_{\max}$ to collide particles at every ion time step. Then, selecting the particles to collide $Nc_{\max}$ times in the entire simulation area, the velocities of these particles are renewed. The postcollision velocities of charged particles are determined by the conservation equations of momentum and energy. The reactions taken into account are elastic scattering, excitation, and ionization for electrons [9-11], and elastic scattering and charge exchange for ions [12].

III. Results and Discussion

Simulations were conducted at the microwave frequency f = 4.0 GHz and the plasma input power P_{in} = 1.0 W, where Xe gas parameters (pressure and gas temperature) were assumed to be spatially uniform and steady (p = 0.5 mTorr and T = 300 K).

Figure 7 shows the two-dimensional distributions of the ion and electron density. Also shown are the applied magnetic field lines. Ions and electrons are generated in the discharge tube area, and flow in to the downstream area with the high density area well confined in the magnetic field, implying that the loss near the wall can be reduced by the magnetic field.

Figure 8 shows the electron temperature and velocities in the z, r and θ direction. At the exit of the discharge tube area, the temperature and the velocity are relatively high. This is because the increase of the intensity of the magnetic fields near a ring magnet, which results in the increase of the velocity owing to the conservation of the magnetic moment. In addition, electrons are accelerated for z direction by diverging magnetic fields in the same principle, implying that the electrons accelerated through the expanding magnetic nozzle generate the ambipolar electric field.

Figure 9 shows the distribution of the potential, indicating a potential drop of ~7 V at the plasma generation area by the self-generated ambipolar electric field. In addition, in the expanding magnetic nozzle region, there is a potential drop of 5~6 V. As a result, there is a potential barrier nearby the exit of the discharge tube area, which may

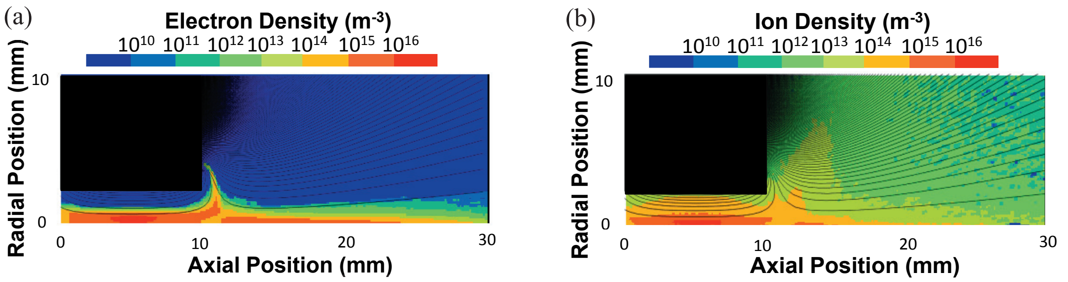

Figure 7. Two-dimensional distributions of the (a) ion and (b) electron density. Also shown are the applied magnetic field lines.

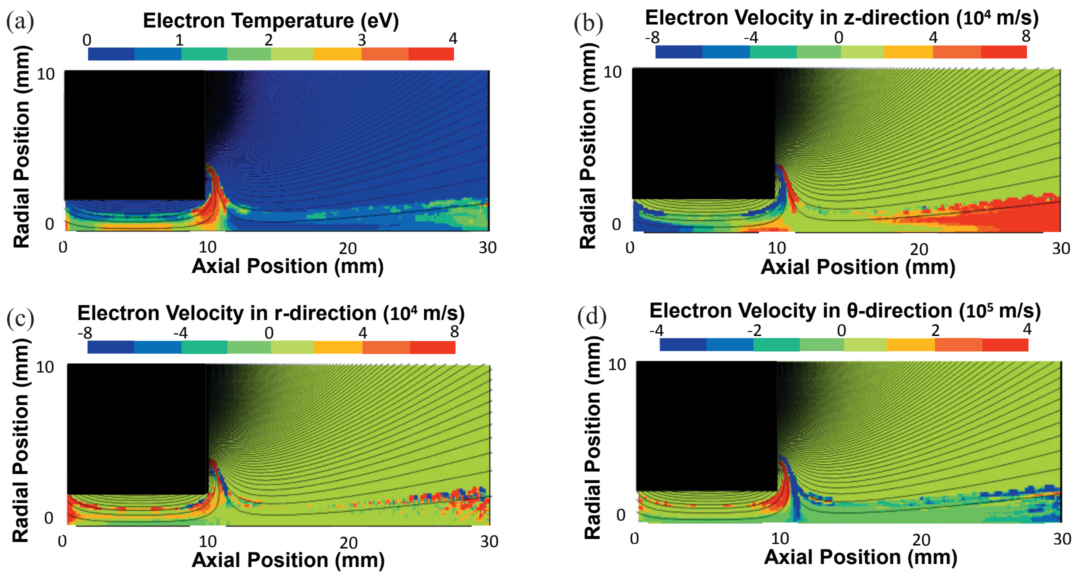

Figure 8. Two-dimensional distributions of the (a) electron temperature, together with those of velocity in the (b) z, (c) r, and (d) θ direction.

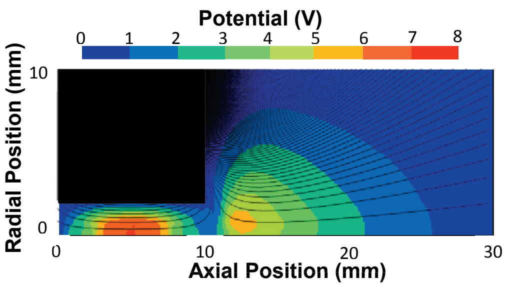

Figure 9. Two-dimensional distribution of the potential.

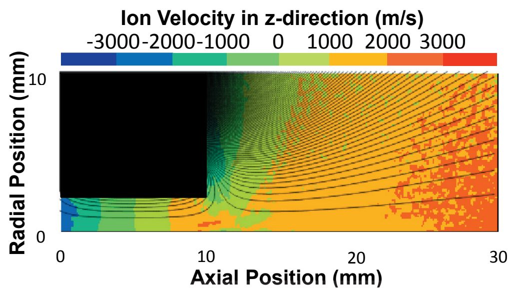

Figure 10. Two-dimensional distributions of the ion velocity in the z-direction.

prevent ions from accelerating smoothly. Figure 10 shows the ion velocity in the z-direction. Ions are accelerated through divergent magnetic fields by the potential drop from < 1000 to > 3000 m/s (< 0.7 to > 6 eV) in the z-direction at $12 < z < 30$ mm. However, ions are decelerated at the exit of the discharge tube area from > 2000 to < 1000 m/s, and thus they are not accelerated continuously. These imply that the modification of the configuration of the permanent magnetic fields is necessary (for example, changing from permanent magnets to a solenoid coils).

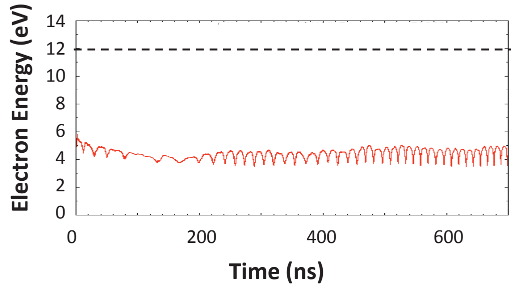

Figure 11. Electron energy as a function of time.

In the discharge tube area, the electron heating by ECR effects does not appear. In order to consider for this problem, we traced one electron in the area concerned. Figure 11 shows an example of the electron energy sampled in the discharge tube area (this area includes the ECR layer) at steady state as a function of time. The ionization energy of Xe (12.1 eV) is also described in the figure with a broken line. At the neutral gas pressure of 0.5 mTorr, gas temperature of 300 K, and the electron density of 1×10^{16} m^{-3}, the mean free time of the electron is ~658 ns. Thus, the figure indicates that electrons in the discharge tube area do not gain enough energy to ionize neutral particles effectively by ECR effects between collisions. In order to enhance the ECR effects, the improvement of the way to input microwaves (for example, changing the microwave frequency) is necessary.

IV. Conclusions

We have conducted PIC/MCC simulations for the micro ECR plasma thruster. The thruster had a quartz tube of 4.15 mm in inner diameter, a semi-rigid coaxial cable inserted in the quartz tube, and outer two ring magnets. We investigated plasma characteristics, plasma confinement by magnetostatic fields of permanent magnets, ion acceleration by divergent magnetic fields, and ECR effects for 4 GHz microwaves and 0.143 T magnetic fields. The results indicated that the plasma generated in the discharge tube area is well confined by permanent magnetic fields, implying that the energy loss at the wall can be reduced by magnetic fields.

The potential drop of 5 ~ 6 V appears in the diverging magnetic fields by the self-generated ambipolar electric field, where ions are accelerated from < 1000 to > 3000 m/s (< 0.7 to > 6 eV) in the z direction at $12 < z < 30$ mm. However, it was also found that the ions are decelerated at the exit of the discharge tube area because of the potential barrier. This implies that the modification of the magnetic field configuration is necessary. In addition, on the distribution of the electron temperature and energy as a function of time, the electron heating in the discharge tube area was not confirmed, implying that changing the way to input microwaves is necessary.

References

[1]Kawanabe, T., Takao, Y., Eriguchi, K. and Ono, K.: Microwave-excited Microplasma Thruster with Applied Magnetic Field, 32nd International Electric Propulsion Conference, 2011, IEPC-2011-262.

[2]Kaneko, T., Hatakeyama, R. and Sato, N.: Potential Formation Triggered by Field-Aligned Electron Acceleration Due to Electron Cyclotron Resonance along Diverging Magnetic-Field Lines, *IEEE Trans. Plasma Sci.*, Vol. 28, 2000, pp. 1747-1754.

[3]Takahashi, K., Oguni, K., Yamada, H. and Fujiwara, T.: Ion acceleration in a solenoid-free plasma expanded by permanent magnets, *Phys. Plasmas*, Vol. 15, 2008, pp. 084501-1-4.

[4]Kousaka, H., and Ono, K.: Numerical Analysis of the Electromagnetic Fields in a Microwave Plasma Source Excited by Azimuthally Symmetric Surface Waves", *Jpn. J. Appl. Phys.*, Vol. 41(4A), Apr 2002, 2199-2206.

[5]Takahashi, T., Takao, Y., Eriguchi, K and Ono, K.: Numerical and experimental study of microwave-excited microplasma and micronozzle flow for a microplasma thruster, *Phys. of Plasmas*, Vol. 16, Aug 2009, 083505.

[6]Takao, Y., Koizumi, H., Komurasaki., K, Eriguchi, K and Ono, K.: Three-dimensional particle-in-cell simulation of a miniature plasma source for a microwave discharge ion thruster, *Plasma Sources Sci. Technol.*, Vol. 23, Dec 2014, 064004.

[7]Peng, Q. L., McMurry, S. M. and Coey, J. M. D.: Axial Magnetic field produced by axially and radially magnetized permanent rings, *J. Magn. Magn. Mater.,* Vol. 268, 2004, pp. 165-169.

[8]Vahedi, V., and Surendra, M.: A monte calro collision model for the particle-in-cell method: application to argon and oxygen discharges, *Comput. Phys. Commun*, Vol. 87, 1995, pp. 179-198.

[9]Hayashi, M.,: Determination of electron-xenon total excitation cross-sections, from threshold to 100 eV, from experimental values of Tounsend's α, *J. Phys. D*, Vol. 16, 1983, pp. 581-589.

[10]Heer, F.J.d, Jansen, R.H.J. and Kaay, W.v.d,:Total Cross Sections for electron scattering by Ne, Ar, Kr and Xe, *J. Phys. B*, Vol. 12, 1979, pp. 979-1002.

[11]Rapp, D and Englander-Golden, P.:Total Cross Sections for Ionization and Attachment in gases by Electron Impact. I. Positive Ionization, *J. Chem. Phys.*, Vol. 43, 1965, pp. 1464-1479.

[12]Boyed, I.D.: Modeling of the near field plume of a Hall thruster, *J. Appl. Phys.*, Vol. 95, 2004, pp. 4575-4584.